nature geoscience

Article

https://doi.org/10.1038/s41561-024-01543-w

Pollution drives multidecadal decline in subarctic methanesulfonic acid

Received: 15 January 2024

Accepted: 22 August 2024

Published online: 23 September 2024

Check for updates

Jacob I. Chalif[1] ✉, Ursula A. Jongebloed[2], Erich C. Osterberg[1], Bess G. Koffman[3], Becky Alexander[2], Dominic A. Winski[4], David J. Polashenski[5], Karen Stamieszkin[6], David G. Ferris[1], Karl J. Kreutz[4], Cameron P. Wake[7] & Jihong Cole-Dai[8]

An industrial-era decline in Greenland ice-core methanesulfonic acid is thought to herald a collapse in North Atlantic marine phytoplankton stocks related to a weakening of the Atlantic meridional overturning circulation. By contrast, stable levels of total marine biogenic sulfur contradict this interpretation and point to changes in atmospheric oxidation as a potential cause of the methanesulfonic acid decline. However, the impact of oxidation on methanesulfonic acid production has not been quantified, nor has this hypothesis been rigorously tested. Here we present a multi-century methanesulfonic acid record from the Denali, Alaska, ice core, which shows a methanesulfonic acid decline similar in magnitude but delayed by 93 years relative to the Greenland record. Box-model results using updated dimethyl sulfide oxidation pathways indicate that oxidation by pollution-driven nitrate radicals has suppressed atmospheric methanesulfonic acid production, explaining most, if not all, of Denali's and Greenland's methanesulfonic acid declines without requiring a change in phytoplankton production. The delayed timing of the North Pacific methanesulfonic acid decline, relative to the North Atlantic, reflects the distinct history of industrialization in upwind regions and is consistent with the Denali and Greenland ice-core nitrate records. These results demonstrate that multidecadal trends in industrial-era Arctic ice-core methanesulfonic acid reflect rising anthropogenic pollution rather than declining marine primary production.

Phytoplankton emit dimethyl sulfide (DMS; CH_3SCH_3), constituting the largest natural source of atmospheric sulfur[1]. After emission, DMS is rapidly converted to several oxidation products, primarily methanesulfonic acid (MSA; CH_3SO_3H) and sulfate, through complex gas- and multi-phase reactions in the atmosphere[2–5] (Fig. 1). MSA is incorporated into aerosols and cloud droplets and is deposited on glaciers and ice sheets, allowing ice cores to serve as long-term archives of atmospheric MSA[6,7]. Ice-core MSA records are typically interpreted to reflect DMS emissions, and thus marine primary production[8–11] and/or sea-ice extent[7,12–14], on the basis of positive correlations between ice-core MSA concentrations and satellite-inferred chlorophyll *a*[10,11,15]. For example, a substantial decline in Greenland ice-core MSA beginning in the mid-nineteenth century has been interpreted to represent a ~10% decline in North Atlantic primary production linked to a weakening of the Atlantic meridional overturning circulation[10]. Such a large drop in marine production would have critical implications for the health of

[1]Department of Earth Sciences, Dartmouth College, Hanover, NH, USA. [2]Department of Atmospheric and Climate Science, University of Washington, Seattle, WA, USA. [3]Department of Geology, Colby College, Waterville, ME, USA. [4]Climate Change Institute and School of Earth and Climate Sciences, University of Maine, Orono, ME, USA. [5]Department of Geosciences, University of Alaska, Fairbanks, AK, USA. [6]Bigelow Laboratory for Ocean Sciences, East Boothbay, ME, USA. [7]Center for North Atlantic Studies, University of New England, Portland, ME, USA. [8]Department of Chemistry and Biochemistry, South Dakota State University, Brookings, SD, USA. ✉e-mail: jacob.ian.chalif@dartmouth.edu

https://doi.org/10.1038/s41561-024-01543-w

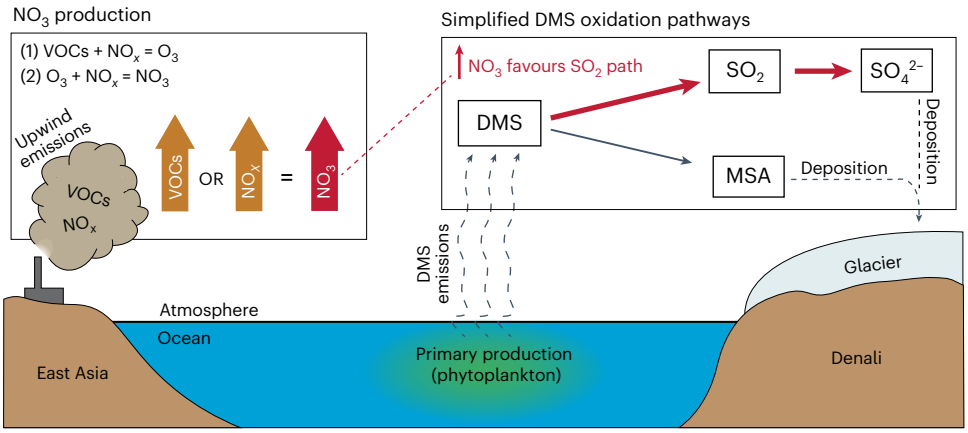

Fig. 1 | Our motivating hypothesis and broad conclusions. Relevant emissions from industrialization, along with reactions that lead to the production of the nitrate radical (NO_3), are on the left. The arrows indicate that increased volatile organic compound (VOC) emissions and/or increased NO_x emissions lead to higher atmospheric NO_3 production. The right-hand panel shows that DMS can be converted to either SO_2 and sulfate (SO_4^{2-}) or MSA before deposition on ice sheets. High NO_3 levels favour the sulfate pathway over the MSA pathway (red arrows).

marine ecosystems[16], the ability of the ocean to sequester carbon[17,18], and global radiative forcing due to the importance of DMS aerosols as cloud condensation nuclei[19–21].

Like most ice-core MSA studies, the interpreted decline in North Atlantic primary production presupposes that the rate of DMS conversion to MSA (and sulfate) is constant over time, implying that the observed decline in atmospheric MSA represents a parallel decline in marine DMS emissions[10]. However, newly published sulfur isotope data from a Greenland ice core contradict the interpretation of a North Atlantic production decline, indicating instead that total biogenic sulfur was 17% higher during the industrial era (IE) relative to the pre-industrial (PI)[22]. Reference 22 hypothesize that anthropogenic changes in atmospheric oxidant concentrations, including nitrogen oxides (NO_x), ozone and reactive halogens, have favoured the oxidative conversion of DMS into sulfate rather than MSA in the IE (Fig. 1). Thus, anthropogenic oxidant emissions may have caused a decrease in atmospheric MSA without a concomitant decrease in phytoplankton DMS emissions.

Anthropogenic changes in atmospheric temperature and oxidant emissions have previously been identified as potential confounding factors in some past ice-core MSA analyses[8,9], but oxidation pathways of DMS are complex and reaction intermediates have only recently been clarified[2–5,23]. Consequently, the impact of anthropogenic emissions on atmospheric MSA concentrations has not been quantified, preventing a rigorous test of this hypothesis until now[7,10,11,15]. Furthermore, if atmospheric oxidants have become the dominant control on MSA levels, one should observe regional differences in the timing of MSA declines that mirror regional differences in anthropogenic oxidant emission histories.

MSA declines in Arctic ice cores

In this Article, we present a 300 year MSA record from the Denali ice core (Alaska, USA) that shows a rapid IE decline in North Pacific MSA similar in magnitude to the North Atlantic decline observed in Greenland ice cores, but delayed by about a century. A Bayesian irregular changepoint analysis[24] identifies 1962 as the highest probability changepoint year when Denali MSA concentrations began to decline after centuries of relative stability since 1700 CE (Fig. 2a and Extended Data Fig. 1a,b). In this analysis, we use the 1962 changepoint as the demarcation between the PI and the IE for the North Pacific source region of the Denali core. During the PI (1700–1961 CE), annualized MSA concentrations were 4.95 ± 1.12 ppb with no notable trend. During the IE (1962–2013 CE), MSA concentrations averaged 3.14 ± 1.08 ppb, representing a decline of 37%.

In the composite Greenland MSA record[10], the Bayesian analysis identifies three changepoints (Fig. 2a and Extended Data Fig. 1c,d): 1854, 1869 and 1953. After the 1854 decline, Greenland MSA levels quickly returned to previous levels by 1862. However, the MSA decline that began in 1869 was the first of a two-step decline that further accelerated in 1953, so we use the 1869 changepoint as the demarcation between the PI and the IE for the North Atlantic source region for Greenland MSA—93 years before the beginning of the North Pacific MSA decline recorded in the Denali ice core. The published Greenland MSA composite record is standardized, with units of *z* scores, making it difficult to quantify the decline in North Atlantic MSA[10]. Therefore, we use MSA from a 2007 ice core drilled at Summit, Greenland[22], hereafter Summit07, to calculate the decline in MSA, using changepoints from the Greenland composite record. In the PI (1767–1868 CE), Greenland MSA levels have no notable trend, with a mean of 2.43 ± 0.47 ppb. Greenland MSA broadly declined throughout the IE (1869–2006 CE), averaging 1.61 ± 0.49 ppb and constituting an MSA decline of 34% from the PI to the IE. This is very similar to the 37% PI to IE decline in North Pacific MSA documented by the Denali ice core.

Regional pollution suppresses downwind MSA production

We incorporated four recently published DMS oxidation mechanisms[2–5] into a box model of gas-phase DMS chemistry (the Framework for 0D (zero dimensional) Atmospheric Modeling (F0AM); Methods) to quantify potential impacts of anthropogenic oxidant emissions on atmospheric MSA in both the North Pacific and North Atlantic. As inputs to the F0AM model, we used atmospheric oxidant concentrations (O_3, OH, HO_2, NO, NO_2, NO_3, BrO and Cl) from PI and IE simulations using GEOS-Chem[25], a global 3D chemical transport model with full HO_x–NO_x–VOC (volatile organic compound)–O_3–halogen–aerosol chemistry[26]. F0AM modelling experiments included an initial concentration of 1 ppb DMS, which was allowed to oxidize away under PI and IE oxidant concentrations output from GEOS-Chem in source regions specific to Denali and Greenland (Extended Data Table 1 and Methods).

In our model experiments, anthropogenic changes in oxidant concentrations resulted in a 27–40% and a 29–50% decrease, respectively, in North Pacific and North Atlantic MSA production due to changes in gas-phase DMS oxidation (Fig. 2b). The four mechanisms for DMS oxidation represent a range of complexity and include different reaction pathways, oxidants and intermediates, yet the model results from all mechanisms show substantial declines in MSA. These results support the hypothesis that higher IE oxidant concentrations favour

https://doi.org/10.1038/s41561-024-01543-w

the oxidation of DMS to form SO_2 and sulfate over MSA. The declines in modelled MSA production are broadly consistent with the observed 37% (Denali) and 34% (Greenland) ice-core MSA declines, suggesting that changes in gas-phase oxidation alone can account for 74–109% (Denali) and 87–149% (Greenland) of the ice-core MSA declines.

The concentrations of all oxidants of DMS have increased in both the Denali and Greenland source regions from the PI to the IE (Extended Data Table 1)[25]. To quantify the role of specific oxidants in the MSA decline, we conducted simulations in which the concentration of one oxidant (or temperature) was held constant from the PI to the IE, while all other parameters were allowed to change (Extended Data Fig. 2). These simulations indicate that increases in NO_3 can largely account for the observed declines in MSA in the North Pacific and North Atlantic (Fig. 2c). In the Denali source region, modelled atmospheric NO_3 concentrations increased by 0.20 ppt from the PI to the IE (a 1,151% increase from the PI), and in the Greenland source region, modelled NO_3 increased by 0.45 ppt from the PI to the IE (a 451% increase). These estimates of PI–IE atmospheric NO_3 increase are smaller than those of similar studies[27,28], suggesting that our model results are a conservative estimate of the NO_3-induced decline in MSA production in the IE compared with the PI. Even with this conservative estimate, the increase in NO_3 alone is responsible for virtually all of the MSA decline in the North Pacific and North Atlantic in our model results.

The increase in NO_3 is the only anthropogenic oxidant change that leads to a substantial decline in MSA production in our modelling experiments. Thus, without an increase in NO_3, model results indicate that atmospheric MSA production would have increased by 2–18% and 10–32% from the PI to the IE in the Denali and Greenland source regions, respectively, due primarily to increases in atmospheric O_3, OH, HO_2 and BrO (Extended Data Fig. 2).

We also investigated the role of anthropogenic warming on atmospheric MSA production by comparing MSA changes in the F0AM model with all oxidant changes but with and without IE warming. We found that warming temperatures, and the resultant impact on the rates of atmospheric chemical reactions, play only a minor role in suppressing MSA production in the IE (Fig. 2c). Detailed box-model sensitivity tests confirm that our results are consistent regardless of the exact PI and IE temperature and oxidant concentration incorporated, within plausible ranges (Methods and Extended Data Figs. 4 and 5).

Our hypothesis that anthropogenic NO_3 emissions are largely responsible for recent MSA trends is supported by the 93 year difference in the onset of the MSA decline in the North Atlantic versus the North Pacific. Atmospheric NO_3 concentrations are controlled by NO_x and VOC emissions[29]. The 1962 decline in Denali MSA is contemporaneous with the onset of increased upwind NO_x emissions from East Asia (Fig. 3a), and the 1869 decline in Greenland MSA parallels the earlier onset of VOC emissions from Western Europe and North America[30]. East Asian emissions of NO_x and VOCs remained low before the mid-twentieth century and then rapidly increased through the present (Fig. 3b). Increases in anthropogenic emissions of NO_x and VOCs from Western Europe and North America began as early as the first half of the nineteenth century and rapidly increased in the mid-twentieth century. Our analysis suggests that this early emission of NO_x and VOCs in Europe and the United States may have contributed to the initial decline in Greenland MSA beginning in 1869. Likewise, the acceleration in emissions of both NO_x and VOCs during the mid-twentieth century in Western Europe and North America coincided with the accelerated decline in Greenland MSA beginning in 1953.

The difference in timing of North Pacific versus North Atlantic NO_x emissions is further reflected by Denali and Greenland ice-core dissolved nitrate (NO_3^-) records, which broadly mirror regional NO_x emissions (Fig. 3). While ice-core NO_3^- records can be affected by post-depositional loss and redistribution in low-accumulation areas[31,32], higher accumulation sites such as Greenland and especially Denali are less affected by this process and better record long-term

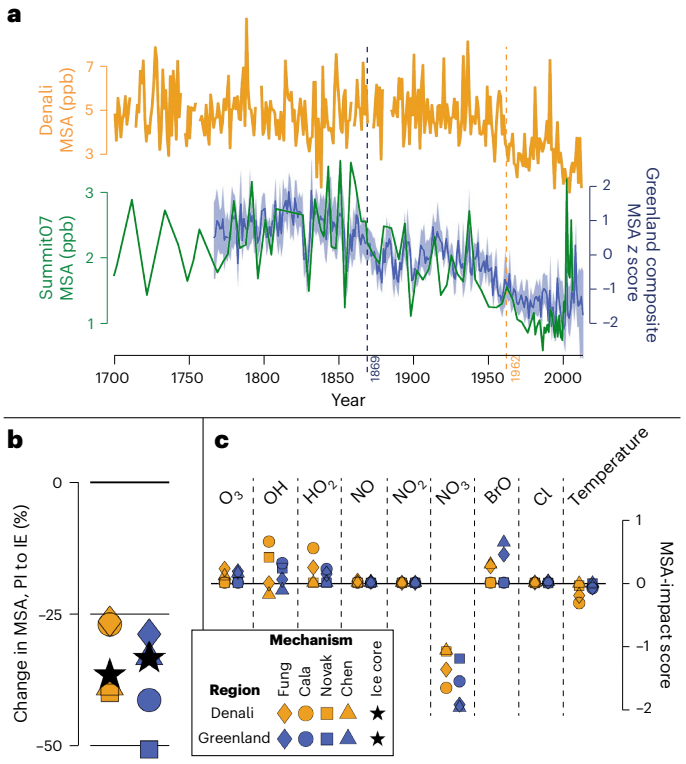

Fig. 2 | Ice-core MSA records alongside F0AM box-model results examining PI–IE DMS oxidation changes. a, Denali (orange), Summit07 (green) and Greenland composite (blue) MSA records. The Greenland composite record is based on MSA from 12 ice cores spanning the Greenland Ice Sheet, with the record's 50th percentile (dark blue) and 95% confidence interval (light blue) given[10]. The composite record shows *z* scores relative to an 1826–2013 baseline. The PI–IE demarcations are shown as vertical dashed lines for Denali (1962, in orange) and Greenland (1869, in blue). **b**, The F0AM-modelled PI–IE percentage change in MSA in the Denali source region (orange) and the Greenland source region (blue). The different shapes represent the DMS oxidation mechanisms tested. The black stars show the measured decline in MSA from ice cores. **c**, The individual impact of each parameter (temperature and oxidants) on MSA production. This was calculated through F0AM model runs in which all parameters changed from the PI to the IE, except for one that was held at PI levels. The 'MSA-impact score' represents the fraction change between the MSA PI–IE change in this scenario and the MSA PI–IE change in **b**. The magnitude of the MSA-impact score represents the oxidative effect of the increase of each parameter from the PI to the IE, with positive values indicating that the oxidant change bolstered MSA production and negative values indicating that the oxidant change suppressed MSA production.

trends in NO_3^- concentrations[32–34] (Supplementary Discussion). Together, the ice core and modelling results indicate that industrial emissions of NO_x and VOCs had a substantial effect on DMS oxidation chemistry, such that atmospheric MSA trends in the North Pacific and North Atlantic are decoupled from DMS trends over multidecadal timescales.

Our model results have two limitations that future research should address. First, DMS oxidation chemistry is an active area of research, and while each of the mechanisms we tested yielded an IE decline in MSA, it is possible that future work on the formation rate and fate of DMS oxidation intermediates may affect these results[2–5,23,35]. In addition, the magnitude of MSA decline is sensitive to the precise PI and IE oxidant concentrations, which are uncertain and difficult to constrain[26,36]. Second, we are including only gas-phase chemistry, but aqueous- and multi-phase chemistries can also be important to the production and loss of MSA[5]. It is possible that uncertain or unknown aqueous-phase reactions of DMS oxidation intermediates could contribute to or offset

https://doi.org/10.1038/s41561-024-01543-w

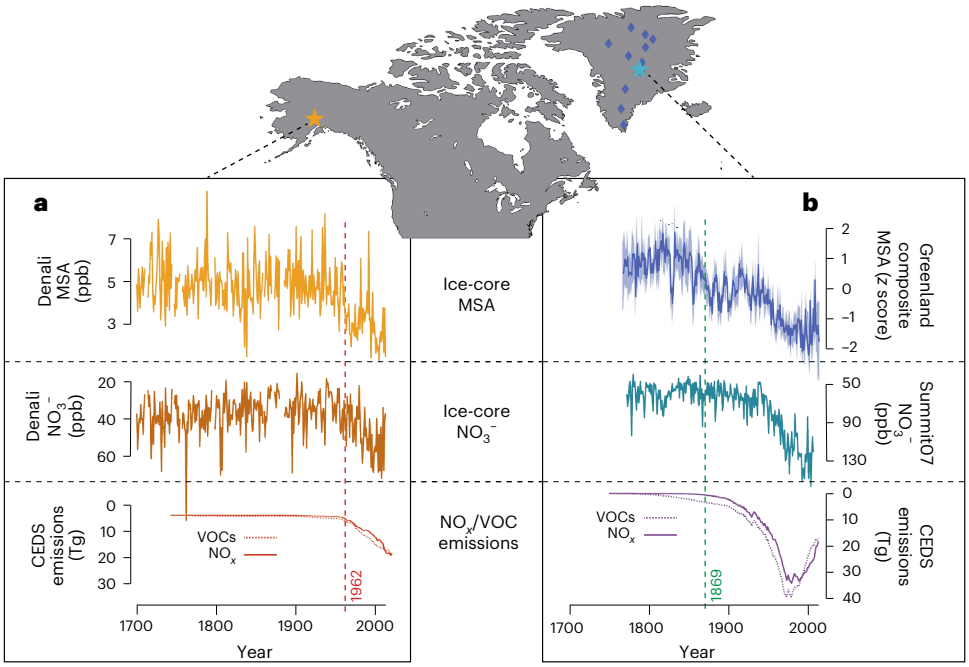

Fig. 3 | Ice-core MSA records alongside oxidant precursor emissions. a, Denali ice-core MSA, Denali ice-core NO_3^- and Community Emissions Data System (CEDS) annual emissions of NO_x (solid) and VOCs (dashed) from East Asia[30]. The 1962 demarcation between the PI and IE for Denali is indicated by a dashed red line. **b**, Greenland MSA composite record, with the record's 50th percentile (dark blue) and 95% confidence interval (light blue) given[10], Summit07 NO_3^- (ref. 49) and CEDS annual emissions of NO_x (solid) and VOCs (dashed) from Western Europe and North America. The 1869 demarcation between the PI and IE for Greenland is indicated by a dashed green line. The locations of the Denali (orange star), Summit07 (teal star) and all Greenland composite (blue diamonds) ice cores are shown at the top. See Supplementary Fig. 3 for a map of the CEDS reference regions.

trends in MSA production, especially if they are sensitive to oxidant concentrations and atmospheric acidity[37–39].

A reinterpretation of IE MSA trends

Beyond the implications for Arctic marine production trends, our interpretation that industrial NO_x and VOC emissions dominate recent MSA changes also has implications for Arctic sea-ice trends inferred from atmospheric MSA. Depending on local sea-ice dynamics, sea-ice extent has been variously interpreted to either positively correlate with primary production and marine DMS emissions through higher nutrient delivery[7–9], or negatively correlate with DMS emissions through declines in production due to light limitation and/or reductions in ocean–atmosphere DMS exchange from ice cover[9,11,40]. Studies that use MSA concentration as a proxy for sea-ice extent, like studies that use MSA as a proxy for productivity, are based on the assumption that the DMS-to-MSA branching ratio remains constant over time. Our results, however, suggest that correlations between MSA and Arctic sea-ice extent in the IE are confounded by the anthropogenic emission of atmospheric oxidants, which suppress MSA production. In a Svalbard ice core, for example, MSA was negatively correlated with sea-ice extent pre-1920, but positively correlated with sea-ice extent post-1920[9], a reversal that could be due to the onset of emissions-induced oxidant suppression of MSA near Svalbard. Likewise, an increase in atmospheric MSA across the Arctic after 1998, previously interpreted to result from sea-ice declines that fostered growth in primary production[40], could reflect declines in NO_x emissions (Fig. 3), which tilt the branching ratio back towards MSA, following stricter environmental regulations.

Our hypothesis helps explain why ice-core MSA has generally been a more reliable sea-ice and productivity proxy in Antarctica than in the Arctic[41]. Whereas it has traditionally been hypothesized that Antarctic MSA is fundamentally easier to interpret than Arctic MSA due to the continent's symmetric sea-ice regime[41], our results suggest that the higher prevalence of anthropogenic pollution in the Northern Hemisphere confounds Arctic MSA records. The concentration of nitrate radicals in the Arctic has increased by an order of magnitude since industrialization, but it has changed only minimally near Antarctica[27,28]. Therefore, modern trends in atmospheric MSA recorded in Antarctic ice cores are able to record changes in productivity or sea-ice extent more robustly than is possible in Arctic ice cores (Extended Data Fig. 2).

Although our results provide an explanation for decreasing atmospheric MSA concentrations independent of marine primary production, abundant satellite[42–44] and in situ measurements[45,46] support the existence of a modern decline in primary production in many parts of the world's oceans. In addition, satellite data show that year-to-year variability in regional primary production is sometimes correlated with Arctic ice-core MSA[7,10,15]. However, our analysis suggests that multidecadal MSA variability in the industrial age is dominated by changes in DMS oxidation to MSA and other sulfur compounds, rather than changes in marine production. The DMS source region of the Denali ice core[15], for example, is within an area that is thought to have experienced an increase in primary production during the second half of the twentieth century[45], despite the contemporaneous decline in atmospheric MSA recorded in the Denali ice core. Thus our results show that it is inadvisable to use Arctic MSA as a direct proxy for primary production, sea-ice extent or long-term changes in the Atlantic meridional overturning circulation[47,48] over the IE.

Online content

Any methods, additional references, Nature Portfolio reporting summaries, source data, extended data, supplementary information, acknowledgements, peer review information; details of author contributions and competing interests; and statements of data and code availability are available at https://doi.org/10.1038/s41561-024-01543-w.

References

1. Andreae, M. O. Ocean–atmosphere interactions in the global biogeochemical sulfur cycle. *Mar. Chem.* **30**, 1–29 (1990).
2. Fung, K. M. et al. Exploring dimethyl sulfide (DMS) oxidation and implications for global aerosol radiative forcing. *Atmos. Chem. Phys.* **22**, 1549–1573 (2022).
3. Cala, B. A. et al. Development, intercomparison, and evaluation of an improved mechanism for the oxidation of dimethyl sulfide in the UKCA model. *Atmos. Chem. Phys.* **23**, 14735–14760 (2023).
4. Novak, G. A. et al. Rapid cloud removal of dimethyl sulfide oxidation products limits SO_2 and cloud condensation nuclei production in the marine atmosphere. *Proc. Natl Acad. Sci. USA* **118**, e2110472118 (2021).
5. Chen, Q., Sherwen, T., Evans, M. & Alexander, B. DMS oxidation and sulfur aerosol formation in the marine troposphere: a focus on reactive halogen and multiphase chemistry. *Atmos. Chem. Phys.* **18**, 13617–13637 (2018).
6. Weller, R. et al. Postdepositional losses of methane sulfonate, nitrate, and chloride at the European Project for Ice Coring in Antarctica deep-drilling site in Dronning Maud Land, Antarctica. *J. Geophys. Res. Atmos.* **109**, D07301 (2004).
7. Maselli, O. J. et al. Sea ice and pollution-modulated changes in Greenland ice core methanesulfonate and bromine. *Clim. Past* **13**, 39–59 (2017).
8. Legrand, M. et al. Sulfur-containing species (methanesulfonate and SO_4) over the last climatic cycle in the Greenland Ice Core Project (central Greenland) ice core. *J. Geophys. Res. Oceans* **102**, 26663–26679 (1997).
9. Isaksson, E., Kekonen, T., Moore, J. & Mulvaney, R. The methanesulfonic acid (MSA) record in a Svalbard ice core. *Ann. Glaciol.* **42**, 345–351 (2005).
10. Osman, M. B. et al. Industrial-era decline in subarctic Atlantic productivity. *Nature* **569**, 551–555 (2019).
11. Kurosaki, Y., Matoba, S., Iizuka, Y., Fujita, K. & Shimada, R. Increased oceanic dimethyl sulfide emissions in areas of sea ice retreat inferred from a Greenland ice core. *Commun. Earth Environ.* **3**, 327 (2022).
12. Curran, M. A. J., van Ommen, T. D., Morgan, V. I., Phillips, K. L. & Palmer, A. S. Ice core evidence for Antarctic sea ice decline since the 1950s. *Science* **302**, 1203–1206 (2003).
13. Welch, K. A., Mayewski, P. A. & Whitlow, S. I. Methanesulfonic acid in coastal Antarctic snow related to sea-ice extent. *Geophys. Res. Lett.* **20**, 443–446 (1993).
14. Criscitiello, A. S. et al. Marine aerosol records of Arctic sea-ice and polynya variability from New Ellesmere and Devon Island firn cores, Nunavut, Canada. *J. Geophys. Res. Oceans* **126**, e2021JC017205 (2021).
15. Polashenski, D. J. et al. Denali ice core methanesulfonic acid records North Pacific marine primary production. *J. Geophys. Res. Atmos.* **123**, 4642–4653 (2018).
16. Lotze, H. K. et al. Global ensemble projections reveal trophic amplification of ocean biomass declines with climate change. *Proc. Natl Acad. Sci. USA* **116**, 12907–12912 (2019).
17. Falkowski, P. G., Barber, R. T. & Smetacek, V. Biogeochemical controls and feedbacks on ocean primary production. *Science* **281**, 200–206 (1998).
18. Wilson, J. D. et al. The biological carbon pump in CMIP6 models: 21st century trends and uncertainties. *Proc. Natl Acad. Sci. USA* **119**, e2204369119 (2022).
19. Carslaw, K. S. et al. Large contribution of natural aerosols to uncertainty in indirect forcing. *Nature* **503**, 67–71 (2013).
20. O'Dowd, C. D. & de Leeuw, G. Marine aerosol production: a review of the current knowledge. *Phil. Trans. R. Soc. A* **365**, 1753–1774 (2007).
21. Park, K.-T. et al. Dimethyl sulfide-induced increase in cloud condensation nuclei in the Arctic atmosphere. *Glob. Biogeochem. Cycles* **35**, e2021GB006969 (2021).
22. Jongebloed, U. A. et al. Industrial-era decline in Arctic methanesulfonic acid is offset by increased biogenic sulfate aerosol. *Proc. Natl Acad. Sci. USA* **120**, e2307587120 (2023).
23. Veres, P. R. et al. Global airborne sampling reveals a previously unobserved dimethyl sulfide oxidation mechanism in the marine atmosphere. *Proc. Natl Acad. Sci. USA* **117**, 4505–4510 (2020).
24. Zhao, K. et al. Detecting change-point, trend, and seasonality in satellite time series data to track abrupt changes and nonlinear dynamics: a Bayesian ensemble algorithm. *Remote Sens. Environ.* **232**, 111181 (2019).
25. Bey, I. et al. Global modeling of tropospheric chemistry with assimilated meteorology: model description and evaluation. *J. Geophys. Res. Atmos.* **106**, 23073–23095 (2001).
26. Wang, X. et al. Global tropospheric halogen (Cl, Br, I) chemistry and its impact on oxidants. *Atmos. Chem. Phys.* **21**, 13973–13996 (2021).
27. Khan, M. A. H. et al. Global modeling of the nitrate radical (NO_3) for present and pre-industrial scenarios. *Atmos. Res.* **164–165**, 347–357 (2015).
28. Karset, I. H. H. et al. Strong impacts on aerosol indirect effects from historical oxidant changes. *Atmos. Chem. Phys.* **18**, 7669–7690 (2018).
29. Archer-Nicholls, S., Allen, R., Abraham, N. L., Griffiths, P. T. & Archibald, A. T. Large simulated future changes in the nitrate radical under the CMIP6 SSP scenarios: implications for oxidation chemistry. *Atmos. Chem. Phys.* **23**, 5801–5813 (2023).
30. Hoesly, R. M. et al. Historical (1750–2014) anthropogenic emissions of reactive gases and aerosols from the Community Emissions Data System (CEDS). *Geosci. Model Dev.* **11**, 369–408 (2018).
31. Frey, M. M., Savarino, J., Morin, S., Erbland, J. & Martins, J. M. F. Photolysis imprint in the nitrate stable isotope signal in snow and atmosphere of East Antarctica and implications for reactive nitrogen cycling. *Atmos. Chem. Phys.* **9**, 8681–8696 (2009).
32. Shi, G. et al. Investigation of post-depositional processing of nitrate in East Antarctic snow: isotopic constraints on photolytic loss, re-oxidation, and source inputs. *Atmos. Chem. Phys.* **15**, 9435–9453 (2015).
33. Fibiger, D. L., Hastings, M. G., Dibb, J. E. & Huey, L. G. The preservation of atmospheric nitrate in snow at Summit, Greenland. *Geophys. Res. Lett.* **40**, 3484–3489 (2013).
34. Fibiger, D. L. et al. Analysis of nitrate in the snow and atmosphere at Summit, Greenland: chemistry and transport. *J. Geophys. Res. Atmos.* **121**, 5010–5030 (2016).
35. Berndt, T., Hoffmann, E. H., Tilgner, A., Stratmann, F. & Herrmann, H. Direct sulfuric acid formation from the gas-phase oxidation of reduced-sulfur compounds. *Nat. Commun.* **14**, 4849 (2023).
36. Zhai, S. et al. Anthropogenic influence on tropospheric reactive bromine since the pre-industrial: implications for Arctic ice-core bromine trends. *Geophys. Res. Lett.* **51**, e2023GL107733 (2024).
37. Mungall, E. L., Wong, J. P. S. & Abbatt, J. P. D. Heterogeneous oxidation of particulate methanesulfonic acid by the hydroxyl radical: kinetics and atmospheric implications. *ACS Earth Space Chem.* **2**, 48–55 (2018).
38. Kwong, K. C. et al. Chemical transformation of methanesulfonic acid and sodium methanesulfonate through heterogeneous OH oxidation. *ACS Earth Space Chem.* **2**, 895–903 (2018).
39. Pye, H. O. T. et al. The acidity of atmospheric particles and clouds. *Atmos. Chem. Phys.* **20**, 4809–4888 (2020).
40. Sharma, S. et al. Influence of transport and ocean ice extent on biogenic aerosol sulfur in the Arctic atmosphere. *J. Geophys. Res. Atmos.* **117**, D12209 (2012).

41. Abram, N. J., Wolff, E. W. & Curran, M. A. J. A review of sea ice proxy information from polar ice cores. *Quat. Sci. Rev.* **79**, 168–183 (2013).
42. Gregg, W. W. & Conkright, M. E. Decadal changes in global ocean chlorophyll. *Geophys. Res. Lett.* **29**, 1730 (2002).
43. Polovina, J. J., Howell, E. A. & Abecassis, M. Ocean's least productive waters are expanding. *Geophys. Res. Lett.* **35**, L03618 (2008).
44. Oziel, L., Massicotte, P., Babin, M. & Devred, E. Decadal changes in Arctic Ocean chlorophyll *a*: bridging ocean color observations from the 1980s to present time. *Remote Sens. Environ.* **275**, 113020 (2022).
45. Boyce, D. G., Lewis, M. R. & Worm, B. Global phytoplankton decline over the past century. *Nature* **466**, 591–596 (2010).
46. Wernand, M. R., van der Woerd, H. J. & Gieskes, W. W. C. Trends in ocean colour and chlorophyll concentration from 1889 to 2000, worldwide. *PLoS ONE* **8**, e63766 (2013).
47. Caesar, L., McCarthy, G. D., Thornalley, D. J. R., Cahill, N. & Rahmstorf, S. Current Atlantic meridional overturning circulation weakest in last millennium. *Nat. Geosci.* **14**, 118–120 (2021).
48. Spooner, P. T. et al. Exceptional 20th century ocean circulation in the northeast Atlantic. *Geophys. Res. Lett.* **47**, e2020GL087577 (2020).
49. Geng, L. et al. Nitrogen isotopes in ice core nitrate linked to anthropogenic atmospheric acidity change. *Proc. Natl Acad. Sci. USA* **111**, 5808–5812 (2014).

Methods

Denali ice-core collection and analysis

Two parallel, surface-to-bedrock ice cores (DEN13A and DEN13B) were drilled in May–June 2013 from the summit plateau of Begguya (62° 56′ N, 151° 5′ W, 3,900 m elevation; also known as Mt Hunter) in Denali National Park, Alaska, USA. The Begguya drill site has a very high annual accumulation rate of 1.4 m water equivalent per year (1981–2011) and a low mean annual temperature of −17 °C, supporting high-resolution and well-preserved palaeoclimate records.

The ice cores were continuously sampled using the Dartmouth ice-core melter system, which features an ultra-clean SiC melthead that separates potentially contaminated meltwater from the core surface and pristine meltwater from the core interior. The water from the interior was peristaltically pumped through an Abakus (Klotz) laser particle counter, a liquid conductivity meter, and collected in pre-cleaned vials for chemical analyses, including stable water isotopes, major ions and trace elements[50]. In this study, we use the MSA record measured by capillary ion chromatography (Dionex ICS5000) from DEN13B. We present the record only from DEN13B because DEN13A was sampled going back only to 1866 CE and its MSA levels contain anomalous drops to zero, representing measurement errors. Despite the erroneous signal drops, both cores demonstrate similar declines in overall MSA concentrations (Extended Data Fig. 3).

Seasonal signals in $\delta^{18}O$, sodium (Na^+), ammonium (NH_4^+), magnesium (Mg^{2+}) and dust particles were used to delineate and count annual layers in the Denali ice core back to approximately 800 CE[51,52]. The depth–age scale was validated by the presence of sulfate spikes corresponding with the dates of known volcanic eruptions (for example, Katmai in 1912, Shiveluch in 1856 and Laki in 1783). The record has an annual resolution back to 1700 CE.

MSA changepoint detection

We performed a Bayesian irregular changepoint analysis[24] on the Denali MSA record, as well as a composite MSA record from 12 Greenland ice cores[10], to identify the onset of industrial MSA decline in the North Pacific and North Atlantic regions, respectively. Thus, while we use the same PI and IE language for both regions, the timing of their respective industrial transitions differs by over a century. To prevent high-frequency changes from biasing the changepoint detection algorithm, we performed the changepoint analysis on 3 year smoothed MSA records from Denali and Greenland. The 3 year smoothing distinguishes the Greenland changepoints from the 1816 changepoint in Greenland MSA found previously[10]. The changepoints identified by our method identify changepoint years that are robust in demarcating changes in the long-term trend or mean, rather than step changes lasting a few anomalous years.

DMS oxidation box model

We used F0AM, a MATLAB open-source box model[53], with updated DMS gas-phase oxidation chemistry from four recent DMS oxidation mechanisms[2–5] (Supplementary Tables 1–4), to estimate the amount of MSA produced from DMS in the PI and IE in light of anthropogenic emissions that increased atmospheric oxidant concentrations and temperature. The four mechanisms—Fung[2], Cala[3], Novak[4] and Chen[5]—vary both in overall complexity and in the specific oxidants and intermediates in the reaction pathway. The Fung mechanism includes DMS oxidation by OH (via addition and abstraction), NO_3, BrO and Cl and intermediates such as DMSO (dimethylsulfoxide), MSIA (methanesulfinic acid), MSP (methylthiomethyl peroxide) and HPMTF (hydroperoxymethyl thioformate). The Cala mechanism includes DMS oxidation by OH (via addition and abstraction) and NO_3 and intermediates such as DMSO, MSIA, MSP and HPMTF. The Novak mechanism includes DMS oxidation by OH (via addition and abstraction), NO_3, BrO and Cl and intermediates in the abstraction pathway only (for example, MSP and HPMTF). Finally, the Chen chemistry includes DMS oxidation by OH (via addition and abstraction), NO_3, BrO and Cl and intermediates in the addition pathway only (for example, MSIA and DMSO). Due to the important role that DMS oxidation by NO_3 plays for our study, we note that the Cala and Novak mechanisms include DMS oxidation by NO_3 to form MSP, whereas in the Fung and Chen mechanisms, DMS+NO_3 oxidation forms SO_2 directly.

We used atmospheric oxidant concentrations from PI and IE simulations in GEOS-Chem[25], a global 3D chemical transport model (version 13.2.1) with full HO_x–NO_x–VOC–O_3–halogen–aerosol chemistry, driven by assimilated meteorology from MERRA-2 (Modern-Era Retrospective analysis for Research and Applications, Version 2), to simulate an IE atmosphere using 2013 emissions and a PI atmosphere by using 2013 natural emissions and meteorology and shutting off all anthropogenic emissions[54]. We computed mean March–October area-weighted modelled oxidant concentrations (Extended Data Table 1) within the marine boundary layer (lowest 2 km) of the North Pacific MSA source region for the Denali ice core (50° N to 62° N, 160° W to 130° W)[15] and for the North Atlantic MSA source region for the Greenland ice cores (50° N to 65° N, 60° W to 10° W)[10]. These regions have been determined as MSA source regions through correlations between sub-annual MSA records in the modern era and satellite chlorophyll *a* observations[10,11,15].

We use GEOS-Chem modelled oxidant concentrations in the F0AM box model to estimate how changes to individual oxidant concentrations could affect the amount of MSA produced from DMS in North Atlantic and North Pacific regions. We set an initial concentration of 1.0 ppb DMS and allowed it to oxidize away under PI conditions and under IE conditions to examine the difference in MSA production. DMS has a short atmospheric lifespan of a few minutes to a few hours in our regions of interest, so this experiment aligns with natural processes[2,55]. To ensure full oxidation plays out with all intermediates, we ran the model for 10 days.

We then performed model experiments to constrain the impact of each individual parameter (oxidant concentrations and temperature) on the amount of MSA produced by holding one parameter at the PI level but all others at their IE levels. We calculated the percentage change in MSA from the PI to the IE in this test ($CNST_p$, where p is a parameter; Extended Data Fig. 2), and compared it with the percentage change in MSA from the PI to the IE in the default scenario in which all parameters change from the PI to the IE (APC). We then calculated the fraction change between $CNST_p$ and APC: $(CNST_p - APC)/APC$. The resulting metric is the MSA-impact score.

As oxidation reaction rate is a function of temperature, we examined a variety of historical temperature reconstructions to estimate PI and IE temperatures in the Denali and Greenland source regions (Supplementary Figs. 1 and 2). Specifically, we analysed four surface temperature reconstructions (Berkeley Earth, CRUTEM5, HadCRUT4 and GISTEMP) and 2 m and 850 hPa air temperatures from six reanalyses (NCEP/NCARv1, ERA5, 20 CRv3, JRA-55, MERRA-2 and ERA-20C) over the entire period covered by each reconstruction (see Supplementary Table 5 for model specifications). The reanalyses provide estimates of absolute temperature, while the surface temperature reconstructions provide temperature anomaly. In anomaly space, all temperature reconstructions appear similar within each source region and atmospheric level, with at most ~0.5 K variance before the onset of the satellite era in 1979. The Denali source region has warmed by up to 1.5 K (Supplementary Fig. 1b,d), and the Greenland source region has experienced up to 1 K of warming since 1900 (Supplementary Fig. 2b,d). As there is substantial year-to-year variation, as well as some variation across models, we chose to use conservative increases of 0.5 K in the Greenland source region and 1 K in the Denali source region. The reanalyses show substantially more variation in absolute temperature in each region and level, with a spread of more than 1 K even in the satellite era. As DMS oxidation occurs throughout the lower atmosphere, rather than at a single level, we chose an absolute temperature about halfway between the 2 m temperature and the 850 hPa temperature.

To test the sensitivity of the FOAM model to the PI and IE oxidant concentrations and temperatures, we performed a series of sensitivity tests, all using the Fung mechanism. First, we modelled the PI and IE scenarios under PI temperatures ranging from 274 K to 282 K, which encompass realistic PI temperatures from the 2 m level to the 850 hPa level in both regions (Supplementary Figs. 1 and 2), and with PI–IE temperature increases ranging from 0 K to 2 K. Even under the most extreme of these scenarios, which represent unlikely conditions, the amount of MSA produced varied by under 10% compared with the chosen PI and IE temperatures (Extended Data Figs. 4 and 5). We conclude that the overall interpretations are not sensitive to the exact PI and IE temperatures used.

Similarly, we performed sensitivity testing of the atmospheric oxidant concentrations used in our PI and IE models by varying the PI and IE concentrations one oxidant at a time. The range of PI and IE oxidant concentrations we tested was based on the 10th to 90th percentiles of the gridded GEOS-Chem oxidant concentrations within each source region. Likewise, to test the sensitivity of our results to the percentage change in oxidant concentrations, we tested the 10th to the 90th percentile range of oxidant concentration percentage change from the PI to the IE in each source region.

We found that the change in PI–IE MSA production (Extended Data Figs. 4 and 5) was not notably affected by the range of PI and IE concentrations tested. For all oxidants except NO_3 and BrO, the exact PI and IE concentration used, within these boundaries, affected the percentage change in MSA by less than 5% (Extended Data Figs. 4 and 5). MSA production was slightly sensitive (MSA percentage change varies by up to 35%) to variations in both the NO_3 and BrO PI concentrations and the percentage change in the IE, which is not surprising given our conclusion that NO_3 and BrO increases in the IE play the largest role in mediating MSA trends (Fig. 2c). Higher PI NO_3 concentrations and/or greater changes in the IE lead to increased suppression of MSA production, and other studies modelling PI–IE change in NO_3 (refs. 27,28) show a higher percentage change in each MSA source region than the GEOS-Chem estimates that we used[54], suggesting that our model results are a conservative estimate of the PI–IE change in gas-phase MSA production. Therefore, we conclude that the interpretations of these model results are not sensitive to the exact PI and IE oxidant concentrations used and are a conservative estimate of the effect of modern-day changes in atmospheric chemistry on DMS oxidation.

To compare the responses of Antarctic MSA and Arctic MSA to IE oxidant level changes, we computed mean September–April area-weighted oxidant concentrations within the marine boundary layer (lowest 2 km) of the Ross Sea, Antarctica, region (72° S to 85° S, 165° E to 137° W) and repeated the box-model experiments for this region (Extended Data Fig. 2). Since the Ross Sea MSA change was very low, the Ross Sea MSA-impact score was high for certain oxidants. To correct for this, we calculated 'MSA-delta' ($CNST_p$ – APC), which is less sensitive to sites with lower overall MSA change.

Data availability

Denali ice-core (DEN13A and DEN13B) MSA data are available from the Arctic Data Center (https://doi.org/10.18739/A2Q814T9K). The Greenland MSA composite record is available from ref. 10, and Summit07 MSA data are available from ref. 22. Denali NO_3^- is available at the National Oceanic and Atmospheric Administration (NOAA) palaeoclimatology database (https://doi.org/10.25921/6cpm-kr44), and Summit07 NO_3^- is available from ref. 49. GEOS-Chem output is from ref. 54. CEDS emissions data used in this study are from ref. 30. All data shown in the Main and Extended Data Figures are available at the preceding references or can be recreated following the Code Availability Statement.

Code availability

The FOAM source code can be downloaded from https://github.com/AirChem/FOAM. Gas-phase MSA mechanisms were implemented following reactions listed in Supplementary Tables 1–4. GEOS-Chem source code can be downloaded from https://github.com/geoschem/geos-chem/tree/13.2.1. Code for Bayesian changepoint analysis was modified from the BEAST package (MATLAB version), which can be downloaded from https://github.com/zhaokg/Rbeast.

References

50. Osterberg, E. C., Handley, M. J., Sneed, S. B., Mayewski, P. A. & Kreutz, K. J. Continuous ice core melter system with discrete sampling for major ion, trace element, and stable isotope analyses. *Environ. Sci. Technol.* **40**, 3355–3361 (2006).
51. Osterberg, E. C. et al. The 1200 year composite ice core record of Aleutian Low intensification. *Geophys. Res. Lett.* **44**, 7447–7454 (2017).
52. Winski, D. et al. Industrial-age doubling of snow accumulation in the Alaska Range linked to tropical ocean warming. *Sci. Rep.* **7**, 17869 (2017).
53. Wolfe, G. M., Marvin, M. R., Roberts, S. J., Travis, K. R. & Liao, J. The Framework for 0-D Atmospheric Modeling (F0AM) v3.1. *Geosci. Model Dev.* **9**, 3309–3319 (2016).
54. Jongebloed, U. A. et al. Underestimated passive volcanic sulfur degassing implies overestimated anthropogenic aerosol forcing. *Geophys. Res. Lett.* **50**, e2022GL102061 (2023).
55. Ghahreman, R. et al. Dimethyl sulfide and its role in aerosol formation and growth in the Arctic summer—a modelling study. *Atmos. Chem. Phys.* **19**, 14455–14476 (2019).

Acknowledgements

Retrieval and analysis of the Denali ice core is supported by the National Science Foundation (NSF) Paleo Perspectives on Climate Change Program (P2C2), grants AGS-1204035 (E.C.O.), AGS-1203838 (K.J.K.) and AGS-1203863 (C.P.W.). Denali National Park and Preserve, Polar Field Services and Talkeetna Air Taxi provided aircraft support and field logistical assistance. We thank M. Waszkiewicz, S. Campbell, B. Markle, E. Burakowski, D. Silverstone and T. Godaire for field assistance, and over 25 students for their assistance sampling and analysing the Denali ice cores in the Dartmouth Ice, Climate, and Environment Laboratory. The Denali ice cores were processed at the NSF Ice Core Facility in Denver, Colorado. J.I.C. acknowledges travel support from the Dartmouth Dickey Center. NSF grants PLR-1904128 (B.A.), PLR-2230350 (B.A.) and AGS-2202287 (B.A.) supported analysis of the Summit07 ice core.

Author contributions

J.I.C. and U.A.J. conceived of and carried out this study. E.C.O., B.G.K. and B.A. provided critical guidance and input throughout. E.C.O., K.J.K. and C.P.W. wrote the initial proposal to drill and chemically analyse the Denali ice core. D.G.F. melted the core and, with D.A.W. and E.C.O., developed the timescale. J.C.-D. obtained funding to drill and measure major ions, including MSA and NO_3^-, in the Summit07 ice core. K.S. and B.G.K. developed a set of initial hypotheses for MSA decline, and K.S. and D.J.P. investigated linkages between Denali MSA and North Pacific production. J.I.C. wrote the paper with input from E.C.O., B.G.K. and U.A.J. All authors discussed the results and reviewed the manuscript.

Competing interests

The authors declare no competing interests.

Additional information

Extended data is available for this paper at https://doi.org/10.1038/s41561-024-01543-w.

Supplementary information The online version contains supplementary material available at https://doi.org/10.1038/s41561-024-01543-w.

Correspondence and requests for materials should be addressed to Jacob I. Chalif.

Peer review information *Nature Geoscience* thanks Alex Archibald, M. Anwar Khan and the other, anonymous, reviewer(s) for their contribution to the peer review of this work. Primary Handling Editor: Xujia Jiang, in collaboration with the *Nature Geoscience* team.

https://doi.org/10.1038/s41561-024-01543-w

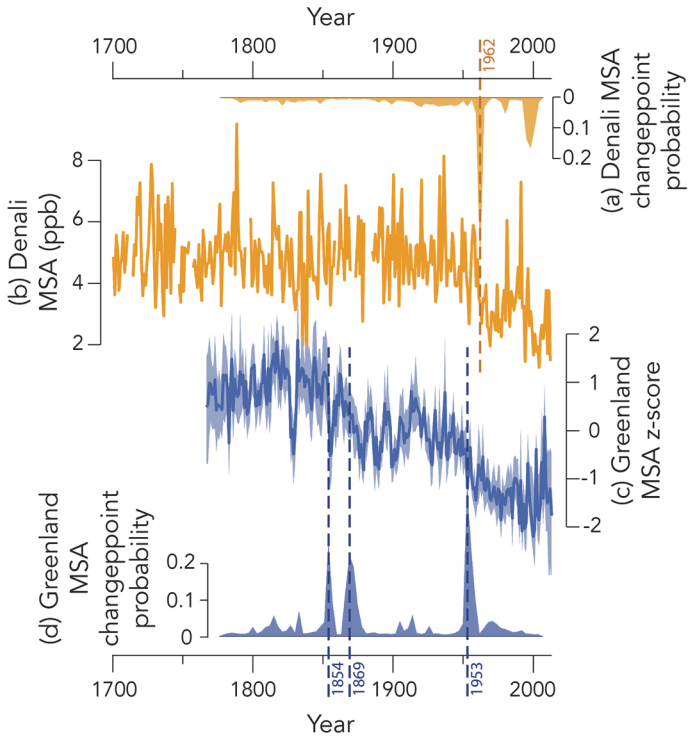

Extended Data Fig. 1 | Ice core MSA records with changepoint probability. (**a**) Denali MSA changepoint probability, based on an irregular Bayesian changepoint analysis (see Methods). The likeliest changepoint year (1962) indicated by a vertical dark orange dashed line. (**b**) Denali MSA. (**c**) The Greenland composite MSA records, with the record's 50th percentile (dark blue) and 95% confidence interval (light blue) given[10]. (**d**) Greenland MSA changepoint probability, with the three likeliest changepoint years (1854, 1869, and 1953) indicated by vertical dark blue dashed lines.

https://doi.org/10.1038/s41561-024-01543-w

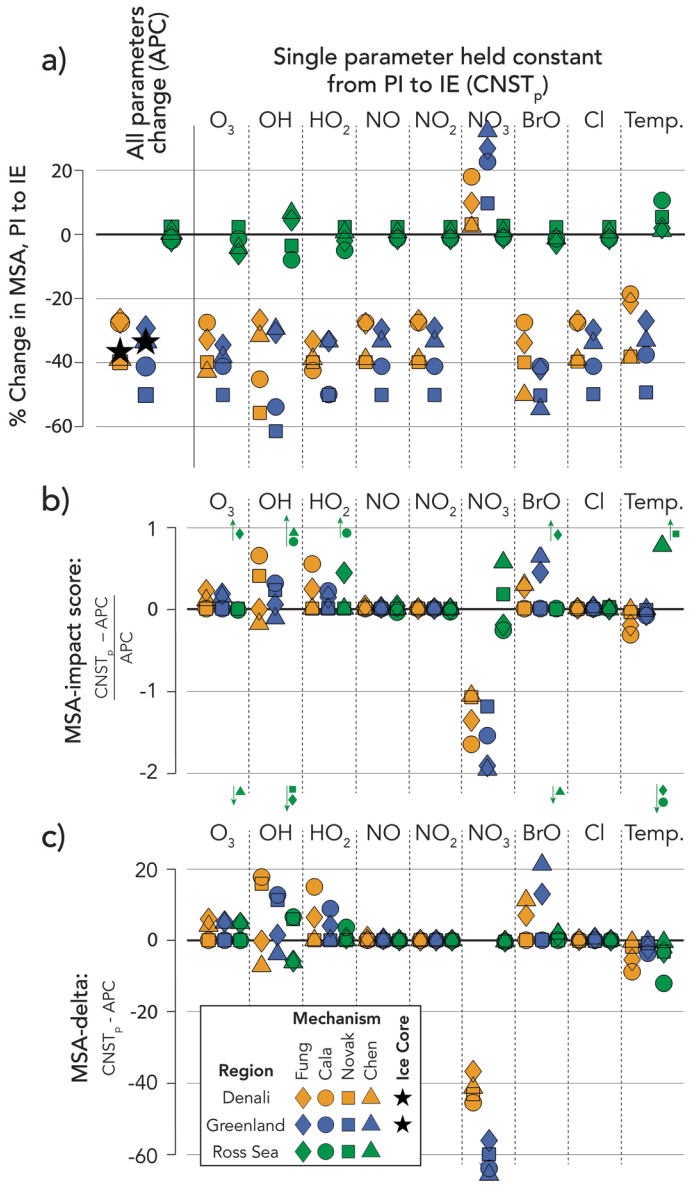

Extended Data Fig. 2 | FOAM box model results, including Ross Sea, Antarctica. (**a**) The PI–IE percent change in MSA under several FOAM model runs, using atmospheric oxidant concentrations from the Denali source region (orange), the Greenland source region (blue), and the Ross Sea, Antarctica (green). The shapes represent the different DMS oxidation mechanisms we used. The APC (leftmost) column shows the change in MSA when all oxidants and temperature (that is, 'parameters') change from the PI to the IE. The columns to the right show the change when one parameter is held constant from the PI to the IE and the rest are allowed to change ($CNST_p$). (**b**) The MSA-impact score, which is the fraction change between $CNST_p$ and APC. The magnitude of the MSA-impact score represents the oxidative effect of the increase of each parameter from the PI to the IE. Note that the impacts of O_3 and OH in the Ross Sea is unusually high because the Ross Sea APC is close to 0. (**c**) An alternative calculation of MSA impact (MSA-delta), calculated by the difference between $CNST_p$ and APC, which corrects the unusually high Ross Sea MSA-impact score in (**b**).

https://doi.org/10.1038/s41561-024-01543-w

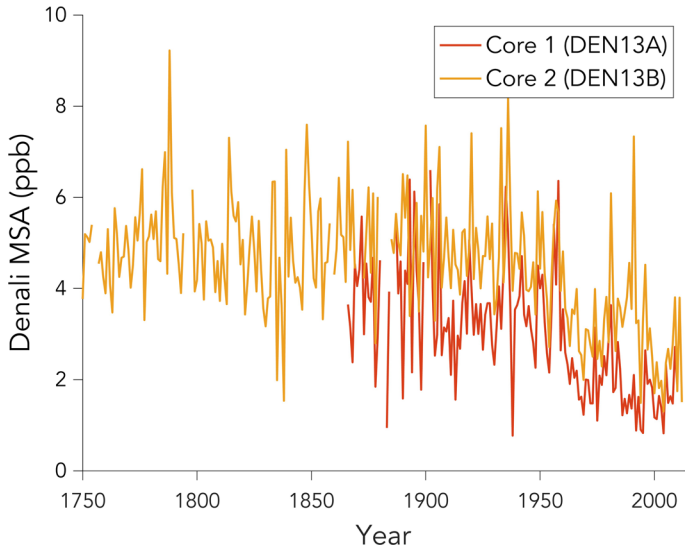

Extended Data Fig. 3 | Denali MSA from cores 1 and 2. The MSA record from Denali core 2 (orange; this study) and core 1 (red). Core 1 was only analyzed to 1866 and its raw record contains anomalous dips to near 0, leading to an overall lower annual average than core 2. Despite the data issues, core 1 contains a mean decline in MSA of 1.79 ppb from 1962–2011 compared with 1866–1961. Core 2, likewise, contains a mean drop of 1.77 ppb over the same period.

https://doi.org/10.1038/s41561-024-01543-w

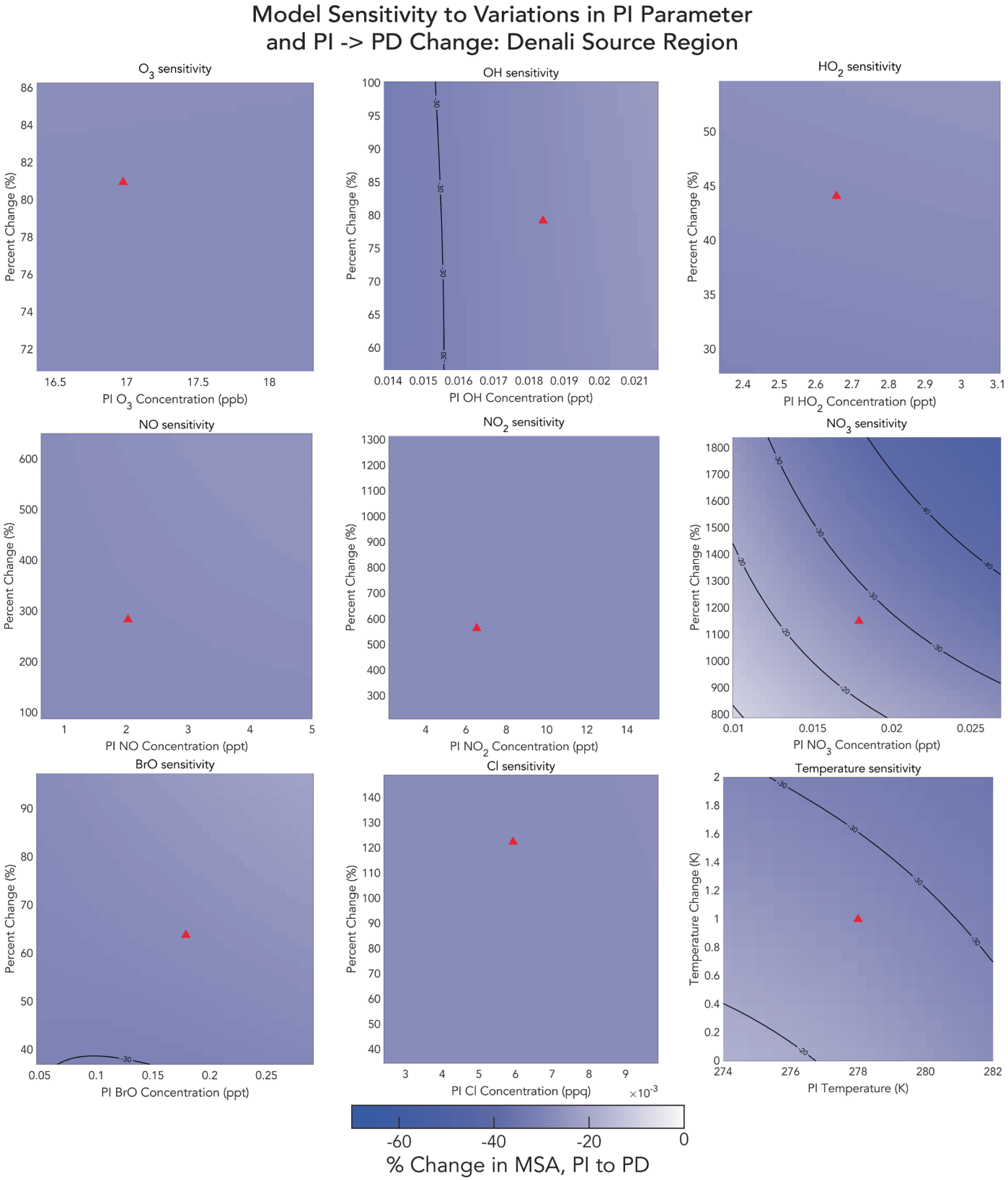

Extended Data Fig. 4 | FOAM model parameter sensitivity testing of the Denali source region. These are model runs in which all parameters (that is, oxidant concentrations and temperature) change from PI to IE, using the Fung mechanism. The red markers indicate the mean modeled changes for the Denali source region. Each panel shows the sensitivity of the model to different selections of the labeled parameter. See Methods for details.

https://doi.org/10.1038/s41561-024-01543-w

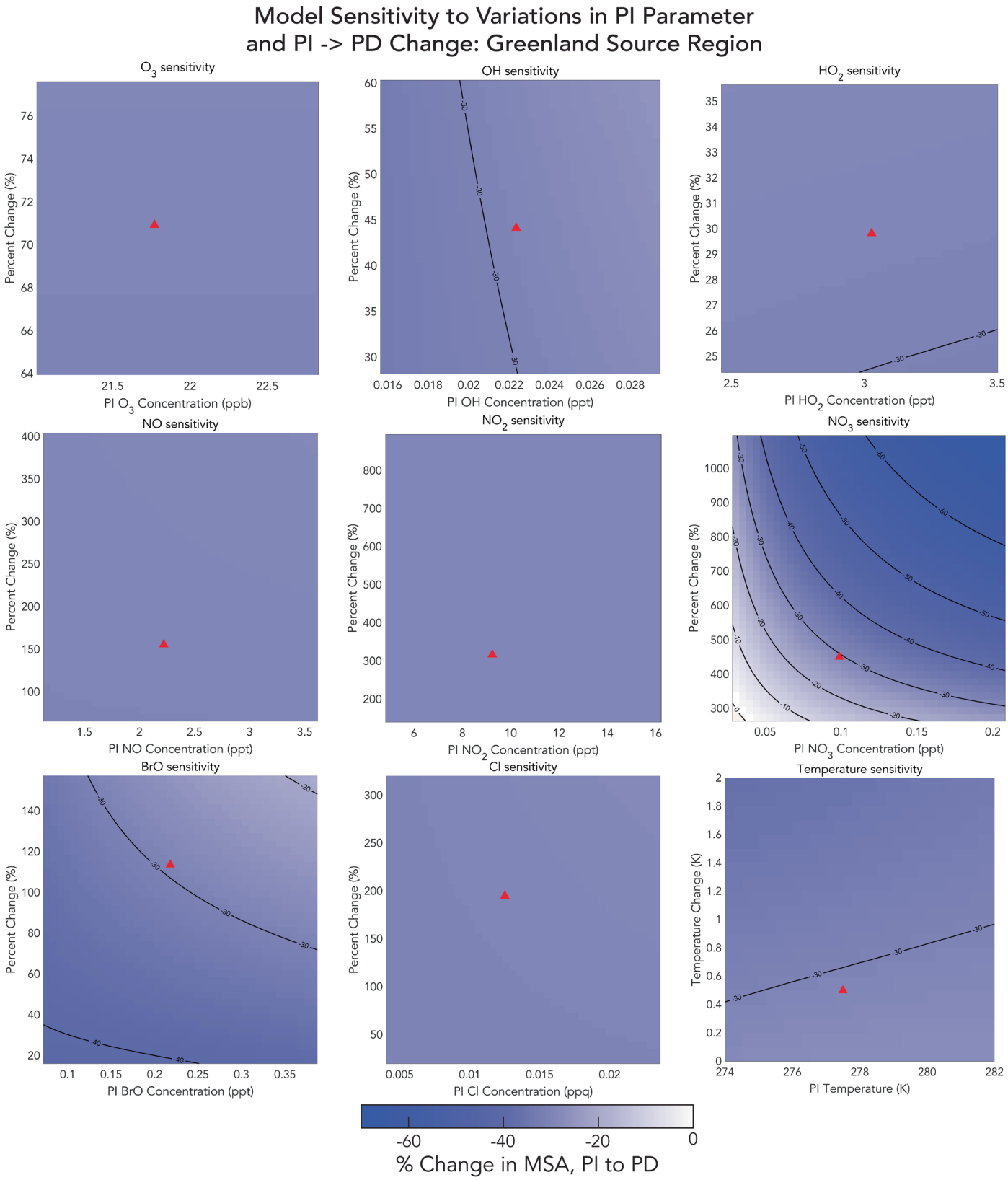

Extended Data Fig. 5 | FOAM model parameter sensitivity testing of the Greenland source region. As with Extended Data Fig. 4, but with the Greenland MSA source region.

https://doi.org/10.1038/s41561-024-01543-w

Extended Data Table 1 | FOAM box model parameters

		Denali Source Region			Greenland Source Region		
Parameter	***Unit***	**PI**	**IE**	**% Change**	**PI**	**IE**	**% Change**
Ozone (O_3)	*ppb*	17	31	81	22	37	68
Hydroxyl radical (OH)	*ppt*	0.02	0.03	79	0.02	0.03	44
Hydroperoxyl radical (HO_2)	*ppt*	2.7	3.8	44	3.0	3.9	30
Nitric oxide (NO)	*ppt*	2.0	7.8	284	2.2	5.7	156
Nitrogen dioxide (NO_2)	*ppt*	6.5	43.4	565	9.2	38.6	317
Nitrate radical (NO_3)	*ppt*	0.02	0.22	1151	0.10	0.55	451
Bromine monoxide radical (BrO)	*ppt*	0.18	0.29	64	0.22	0.47	114
Chlorine radical (Cl)	*ppq*	0.006	0.013	122	0.012	0.037	195